JOURNAL OF AIRCRAFT
Vol. 32, No. 2, March–April 1995

Analysis of Vortex Bursting Utilizing Three-Dimensional Laser Measurements

Kenneth C. Cornelius*
Wright State University, Dayton, Ohio 45435

From the analysis of experimental three-dimensional laser velocimeter data of a vortex burst condition on a generic fighter configuration, a criterion for vortex breakdown has been evaluated. The measured velocity vectors were rotated from the tunnel coordinate system to the vortex core trajectory to examine the relevant parameters for vortex instability. The Rossby parameters that govern stability were formulated in terms of the local vortex flow variables. The ratio of axial-to-crossflow energy evaluated from the data encompassing a region bounded by the vorticity provides for a parameter that is consistent with Ludwieg's spiral instability analysis for conical flow. Benjamin's analysis for supercritical flow transition is correlated with a parameter for the mean flow vortex variables. The magnitudes of the critical parameters decrease downstream from the adverse pressure gradient along the vortex trajectory providing a threshold that correlates with the vortex breakdown position.

Nomenclature

A_v	=	area encompassing viscous subcore
A_ξ	=	area encompassing axial vorticity
C_l	=	lift coefficient
C_m, C_N	=	pitching and yawing moment coefficient
c_{ma}	=	mean aerodynamic chord length, 12.7 cm
c_r	=	root chord of wing, 15.24 cm
L	=	total length of model, 46.43 cm
P	=	static pressure
$P_{t\infty}$	=	freestream total pressure
Q	=	dynamic head
q'	=	turbulence kinetic energy
R_{mr}	=	energy ratio, axial/crossflow
R_{rc}	=	Reynolds number based on root chord
R_Γ	=	Rossby number based on U_c and circulation, Γ_v
r_v	=	radius of viscous subcore
r_ξ	=	equivalent radius of vortex, $\sqrt{(A_\xi/\pi)}$
S	=	swirl velocity ratio
S_m	=	model reference area, 0.0444 m^2
s	=	wingspan, 35 cm
$(U, V, W)_t$	=	mean velocity, tunnel coordinates
(U_x, V_r, V_φ)	=	mean velocity, conical coordinates
$(U, V, W)_\xi$	=	mean velocity, vortex coordinates
$(x, y, z)_\xi$	=	coordinate axis of vortex trajectory
α	=	angle of attack
Γ	=	circulation, $\int\int_{A_\xi} \xi_x \, dA$
Γ_v	=	circulation in viscous subcore $\int\int_{A_v} \xi_x \, dA_v$
Γ^*	=	normalized circulation $(\Gamma/U_\infty c_r)$
ξ_x	=	axial chordwise vorticity
ψ	=	sideslip angle

Subscripts

c	=	centerline of vortex core
e	=	outer edge of vortex core

Introduction

FUTURE air combat will require aircraft maneuver performance that will exceed the capability of present day fighters. At high angles of attack in the poststall region, the aerodynamic control surfaces such as the vertical tail and rudder become engulfed in the separated flowfield of the wing and lose their ability to impart the yawing moment and side force required for active control of the vehicle. Compounding this problem further, the aircraft is susceptible to asymmetrical side forces generated in the vicinity of the apex of the fuselage or nose region beyond a 30–40-deg angle of attack. These forces arise from the bistable nature of the three-dimensional boundary-layer separation around the periphery of the nose, which leads to unequal strength vortices around the forebody. This phenomenon is believed to be caused by a small asymmetry in the fuselage geometry or upstream flow angularity that perpetuates a small perturbation in the flow, and the resultant convective instability amplifies downstream and locks on in one direction. If the flow angularity switches in direction, the vortex flow asymmetry follows suit. At high angles of attack the shear layer emanating from the separation lines of the body or sharp winglets leads to a flowfield dominated by an organized pair of vortical flows that influences the pressure distribution around the forebody. The resulting flowfield leads to an unstable side force and yawing moment, which are detrimental to the controlled motion of the aircraft. This lateral instability must be rectified if poststall multiaxis maneuvering of fighter aircraft is to become a realistic goal.

The flowfield of modern fighters is further complicated by the use of low aspect ratio strakes, i.e., leading-edge extensions (LEX) in front of the main wing, which allows high maneuverability fighters such as the F-16 and F/A-18 to increase the stability range of their operational envelope. The vortices generated from the LEX interact with the main wing flow to enhance lift and provide aerodynamic stability throughout an expanded operational flight regime. However, the extension of the flight envelope to higher angles of attack and the increase of the stall/spin resistance are limited by the onset of vortex breakdown from either of the individual vortex formations and their interactions with the control surfaces. This is a striking phenomenon due to the nature of the abrupt changes in the vortex flow physics that results in the turbulent dissipation of energy and the dramatic increase in the physical boundary of the vorticity. Recently,[1] it has been demonstrated that decoupling of the LEX vortex flow from the wing vortex delays the vortex breakdown and significantly increases the maximum lift. The decoupling was achieved by physically moving the LEX planform above the wing plane, which prevented the strong interaction and the eventual merging of the

Presented as Paper 90-3020 at the AIAA 8th Applied Aerodynamics Conference, Portland, OR, Aug. 20–22, 1990; received April 23, 1993; revision received June 2, 1994; accepted for publication June 3, 1994.

*Associate Professor, Department of Mechanical and Materials Engineering. Senior Member AIAA.

LEX vortex with the wing vortex. The LEX vortex traversed a trajectory closer to the root of the main wing, which provides boundary-layer control and delayed bursting of the vortex to a higher angle of attack.

Roll agility in modern fighters is often limited by the onset of lateral-directional instability at high angle of attack, which is governed in part by the asymmetrical pressure distribution around the periphery of the aircraft nose. By blowing tangentially to the forebody surface on the leeward side of the vortex in the nose region, various investigators[2-5] have demonstrated significant control and aerodynamic enhancement of maneuverability. Both yaw and side force control at high angles of attack can be enhanced by controlling the forebody vortex separation position and strength around the periphery of the nose. Recent experiments[6] have demonstrated that spanwise blowing in the direction of the wing vortex coordinates can influence the vortex breakdown position and extend the range of maximum lift. Recent designs such as the F117A and F22 fighter aircraft have incorporated a chined forebody that is contoured and merged with the wing planform, both for structural reasons and to circumvent the statically unstable yawing moment from the vortex separations of the rounded forebody. However, the strong vortex interactions at high angles of attack, especially when the aircraft is yawed, lead to destabilizing moments. The effects of the vortex burst lead to unstable aerodynamics of the vehicle and are responsible for an adverse or nose-up pitching moment. Another detrimental feature during high angle-of-attack maneuvers is the unsteady vortex wake flow interaction with the vertical stabilizer causing large transient loads on the control surface, which may lead to premature failure of the load bearing structure due to fatigue. It becomes imperative that in order to achieve higher angle-of-attack maneuverability for fighter aircraft, the phenomena of separation-induced vortex flows and the bursting process must be better understood.

The primary research of this article analyzed experimental data for the critical parameters that govern vortex stability. The data was obtained utilizing a three-dimensional laser Doppler velocimeter (LDV). The model configuration was a generic chined-forebody configuration. The data[7] consist of the mean (U, V, and W) velocity components as well as turbulence measurements at various x/c_r locations along the fighter wing geometry at separate angles of attack.

Model and Flow Characteristics

The details of the Generic Fighter model configuration used in this study are shown in Fig. 1. It is constructed from aluminum and has a length of 46.4 cm, a span of 34.9 cm, and a root chord of 15.24 cm. The wing has a leading-edge sweep of 56 deg, and a trailing-edge sweep of 30 deg. The chined forebody has a sweep of 76 deg. The fuselage and wing geometry were blended in such a manner so as to eliminate surface discontinuities, and are therefore considered a blended wing-body configuration. Both the forebody and wing have sharp leading edges that are conducive to a three-dimensional separation leading to strong equal strength vortex flows on either side of the fuselage at high angles of attack. For this configuration the forebody vortex turns abruptly at the wing juncture plane and merges with the separated wing flow vorticity. The vortex flow about the chined forebody and wing geometry leads to favorable aerodynamic characteristics until the resulting flow approaches the breakdown condition that can be categorized as vortex bursting. These data contain a case in which vortex bursting occurs at an angle of attack $\alpha = 21$ deg, with a domain of reverse flow that is characteristic of the "bubble"-type breakdown at an axial location of $x/c_r = 0.59$. At an angle of attack $\alpha = 10$ deg of the model relative to the freestream, there is no reverse flow in the vortex domain, but a significant increase in the core radius downstream.

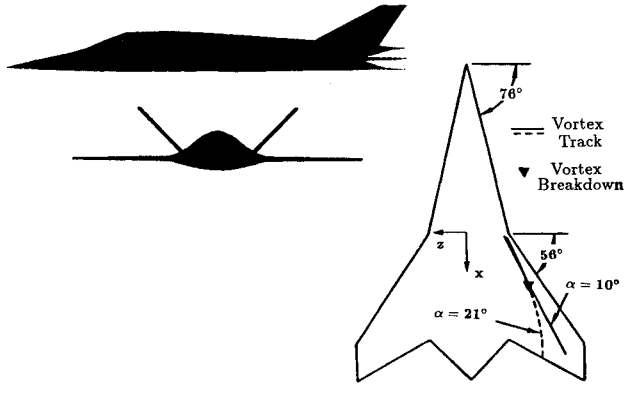

Fig. 1 Two-dimensional view of chined forebody fighter.

Test Facility

The laser test was conducted in a low-turbulence wind tunnel that is fully instrumented and principally dedicated to LDV measurements of the flow velocity about aerodynamic configurations. The facility used in this investigation is a closed-return low-speed wind tunnel powered by a 30-hp motor attached to a four-bladed axial fan. The contraction ratio of 20:1 is preceded by five screens that provide a working section turbulence intensity less than 0.05%. For the three-dimensional study reported below the test section size was 0.91 m high, 0.61 m wide, and 6.0 m in length. The maximum speed utilized in this study was 41.0 m/s. The freestream speed was controlled by monitoring a set of calibrated Piezzio rings installed upstream of the test section. A glass sidewall of the test section provided optical transmission of the laser beams and the scattered light from individual particles for the local measurement of the instantaneous velocity vector. The model was mounted onto a long sting and cantilevered on a circular aluminum turntable on the adjacent wall section of the wind tunnel to facilitate angle-of-attack changes. Due to the sensitivity of model mounting[8,9] and the influence on the vortex flow breakdown, attention was given to extending the sting to the far wake before attachment to the side wall. To minimize the aerodynamic effects the sting of length 1.35 m was tapered to a constant diameter to 2 cm at an axial distance of 0.3 m with the tapered forward section attached to the base of the model. In this geometric arrangement the sting simulated the exhaust flow from the engine in the near wake. Figure 2 shows the model mounting position in the low-speed wind tunnel for the laser data. The wind tunnel is a low-speed facility with a maximum dynamic head [$Q_{max} = 48.4$ N/m^2 (20 psf)], which is ideally suited to laser-velocimeter flowfield measurements. The Reynolds number, based on tunnel free-

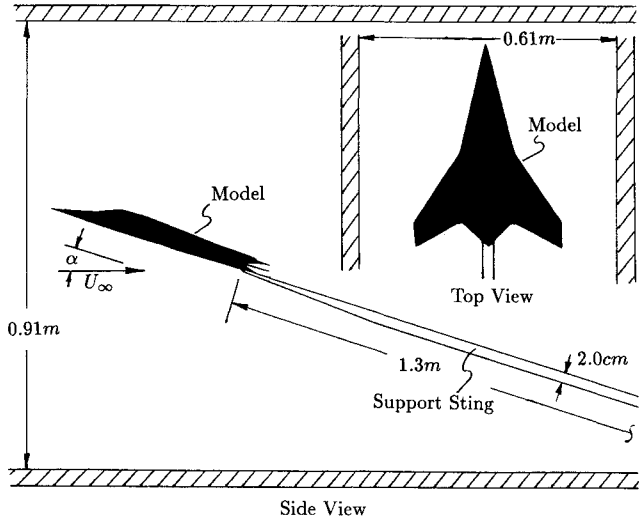

Fig. 2 Model mounting position for laser data.

stream velocity and length along the model centerline, was 1.25×10^6.

Aerodynamic Force Data

For the force measurements the model was placed in a larger tunnel of test section size 1.22 m high, 1.22 m wide, and 2.0 m in length. The lift and pitching moment coefficients of the aircraft configuration are shown in Fig. 3. The first noticeable change in the physics of the vortex flow occurs at 8–10 deg angle of attack of the model. The wing vortex flow becomes unstable near the trailing edge of the wing at these angles and has a significant effect on reversing the slope of the pitching moment C_m, which affects the longitudinal static stability. A nose-up pitching moment commences at an angle of attack of 14 deg. For the sideslip data the basic fighter configuration was retrofitted with two canted vertical tails as shown in Fig. 1. The yawing moment C_N vs ψ with and without the two canted control surfaces is shown in Fig. 4. The yawing moment was referenced to the quarter root chord of the main wing. The tails provide a stabilizing side force and yaw moment. However, beyond 5 deg of sideslip and an angle of attack of 20 deg, a discontinuity and nonlinear trend is apparent from the data. A strong interaction between the vortex flow and the vertical tail is responsible for this trend. Beyond the range of approximately 30 deg of attack the slanted vertical tail control surface is ineffective in providing a restoring yawing moment to the aircraft. These two characteristics limit the flight envelope of the aircraft and constrain the high angle-of-attack maneuverability and agility of the vehicle.

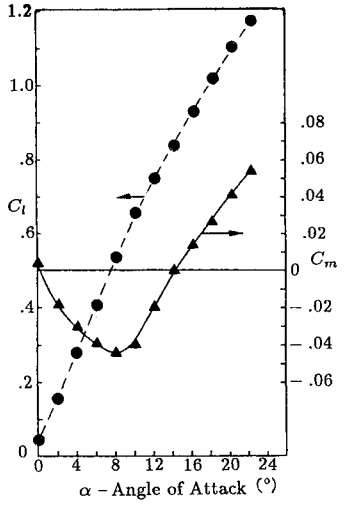

Fig. 3 Lift and pitching moment coefficient.

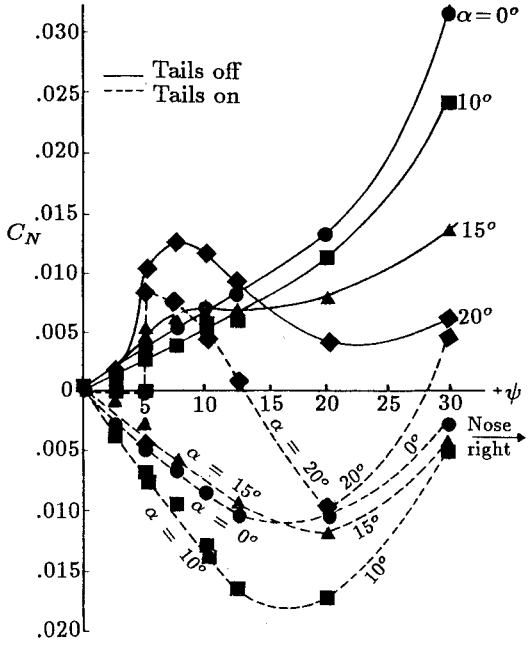

Fig. 4 Yawing moment vs sideslip angle.

Experimental Three-Dimensional Laser Measurements

For the LDV measurements the generic fighter model was rotated about the tunnel centerline to alter the angle-of-attack range up to 21 deg. Three-dimensional velocity measurements were acquired using a three-dimensional LDV system. The (U, V) data were acquired in the conventional manner with an 18-W argon-ion laser providing a blue and green coherent light source. Another 18-W argon-ion laser configured with an internal prism provided the purple coherent light source and was mounted at 45 deg to the freestream to measure the combination of (U, W) components of velocity. The two sets of collection optics operated in the backscatter mode. The bragg cells operated in the 40–48-MHz range that shifted one of each beam pair, and the difference frequency was achieved electronically. A three-dimensional positioning table allowed traversing in the (x, y, z), coordinate directions with a resolution of 0.0025 cm. Figure 5 shows a sketch of the top view of the laser orientation and traverse table. Since the laser Doppler data were configured electronically to be coincident in time, all of the Reynolds stresses were measured, and the W component was extracted instantaneously from the second set of measurements utilizing the geometry of the beams. Each ensemble average represents 1000 data points in a spatial volume of 0.013 cm radius by 0.06 cm length, which was dictated by the focusing and collection optics.

The seeding particles for the LDV were oil droplets 1 μm in diam, and were introduced into the wind-tunnel flowfield through a compressed airline downstream of the model for the purpose of providing scattering cross sections of the laser light throughout the flowfield and the freestream of the closed return tunnel. A table was constructed for the (y, z) coordinates at any desired axial station, and this information was used for automatic traversing of the three-dimensional traverse table. The (y, z) plane where data were obtained was configured to be normal to the axis of the model, i.e., rotated at the angle of attack. The measured velocities (U, V, and W) were obtained in the model coordinate axis. The data was acquired with the vertical tails removed at various x/c_r chordwise positions to assess the development of the streamwise vorticity. The LDV velocity data are presented in the form of contour plots of various quantities such as the mean axial

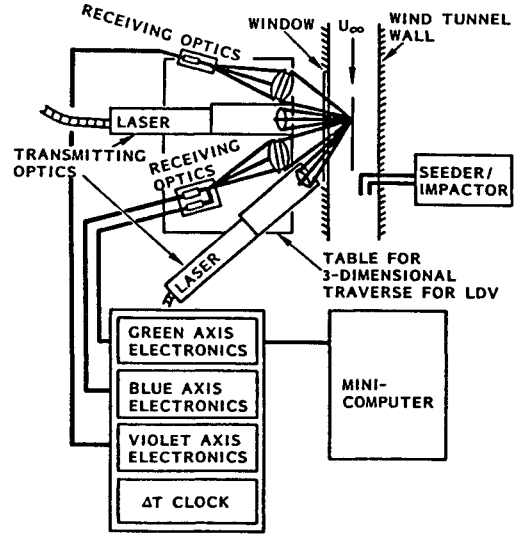

Fig. 5 Planform view of LDV system.

vorticity, axial, and crossflow velocity components, as well as the turbulence kinetic energy. Various parameters were integrated in the core vorticity domain to formulate a Rossby number criterion that shows that there is a critical threshold or condition demonstrating the onset of the breakdown and instability of the vortex flow. These flowfield measurements obtained from a nonintrusive acquisition of the velocity field in the vortex burst region provide a valuable data base for the validation of computational methods.

Data Analysis

The significant differences between the axisymmetric vortex studies generated in a confined tube and delta-wing generated vortices are the boundary conditions. For the sharp delta wing configuration there is a continuous generation of vorticity along the leading edge from the separated shear layer. In a spiraling fashion the shed vorticity feeds continuously into the outer core and, consequently, the circulation of the primary vortex increases along the axis. There is an opposite sense vortical region generated from the three-dimensional separating boundary layer commonly referred to as the secondary vorticity that resides outside the main vortex near the wing surface.

The coordinate system that has relevance to previous theoretical and experimental research in terms of vortex bursting is the coordinate axis along the vortex core. Hence, the $(U, V, W)_t$ velocity components were rotated by the Euler angles (α_v, ψ_v) relative to the orthogonal coordinate system of the wind-tunnel axis to coincide with the trajectory of the center of the core at each chordwise station along the configuration. The trajectory of the core was obtained by software that performed an integration of the vorticity in the measurement plane perpindicular to the axis of the model to determine the average spatial positions (y, z) of the vortex center. A least-square curve fit through these points in the x direction was used to determine the respective Euler angles. The velocity data $(U, V, W)_t$ were transformed to the orthogonal coordinate system along the vorticity core using matrix algebra to produce $(U, V, W)_\xi$.

Crossflow Velocity Vectors and Axial Vorticity

The rotated $(V, W)_\xi$ velocities are shown in Fig. 6 where the length of the vector represents the magnitude of the crossflow component. A well-organized vortical flow and large swirl component is apparent for the 21-deg angle-of-attack case before breakdown of the vortex in the vicinity of $x/c_r \simeq 0.59$. The local vorticity magnitude ξ_{vx} was determined by the use of Stoke's theorem. The numerical value was assigned at the center of each grid cell and normalized by the freestream velocity and root chord of the wing. Figure 7 shows the area increase of the vorticity region A_ξ along the chord for the two angle-of-attack cases. Both angle-of-attack cases show an increase in the vortex area beyond $x/c_r \simeq 0.59$. A_ξ was calculated by summing the cell areas that contained a positive magnitude of ξ_{vx}, 5% above the background noise level. The values were normalized by the respective calculations of the initial vorticity area A_0 at $x/c_r = 0$, which represents the position at the origin of the wing/fuselage juncture. Figure 8 shows the development of the axial vorticity contours along the trajectory of the core. The chined forebody vortex turns abruptly at the wing juncture and merges with the main wing vortex, where two distinct elongated vortical cores are visible at $x/c_r = 0.13$. The chined vortex data is not presented in Fig. 8. For the model oriented at a 21-deg angle of attack, the vortex bursting and the onset of axial flow reversal occurs at an $x/c_r = 0.59$ location. The vorticity is convoluted to a larger physical domain by the turbulence energy producing eddies, which is characteristic of the breakdown process. The circulation in the half-plane was determined by integrating the positive vorticity throughout the measurement domain. Figure 9 shows the dimensionless positive circulation Γ vs the chordwise axial

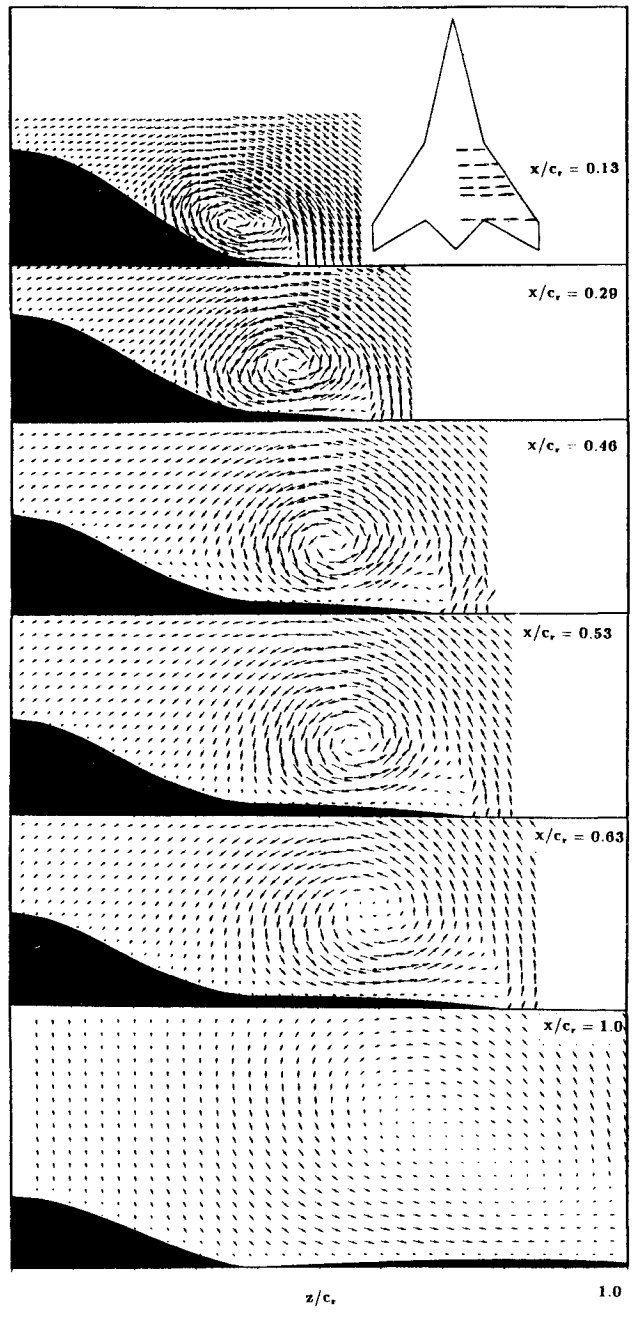

Fig. 6 V-W vectors at $\alpha = 21$ deg.

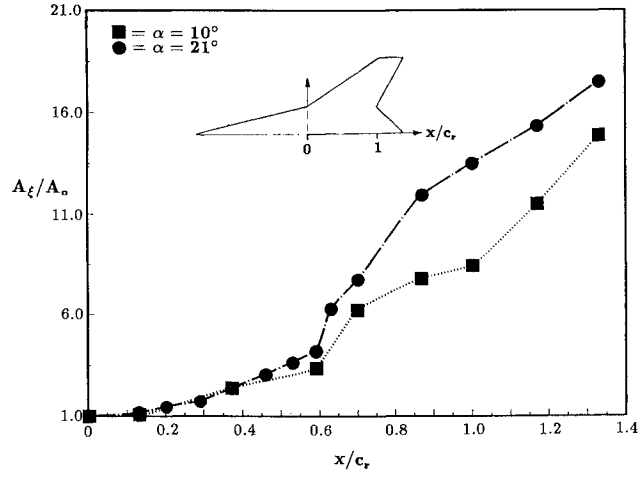

Fig. 7 Area enclosed by positive chordwise vorticity.

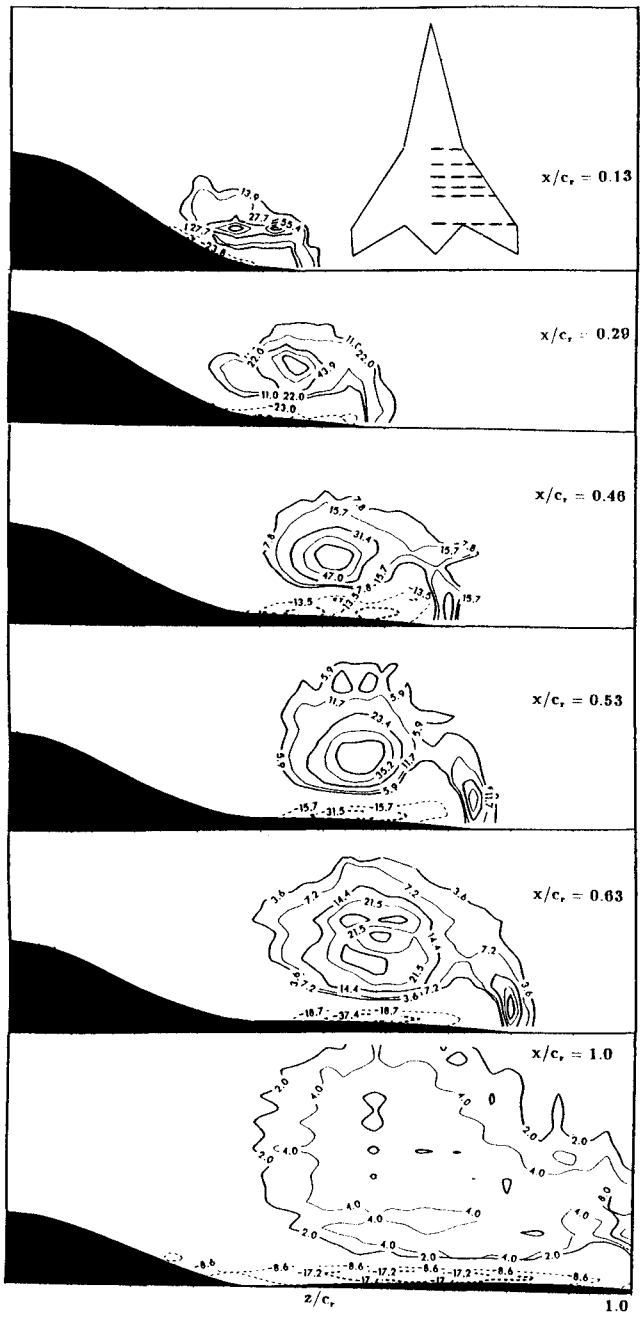

Fig. 8 Chordwise vorticity contours ξ_x at α = 21 deg.

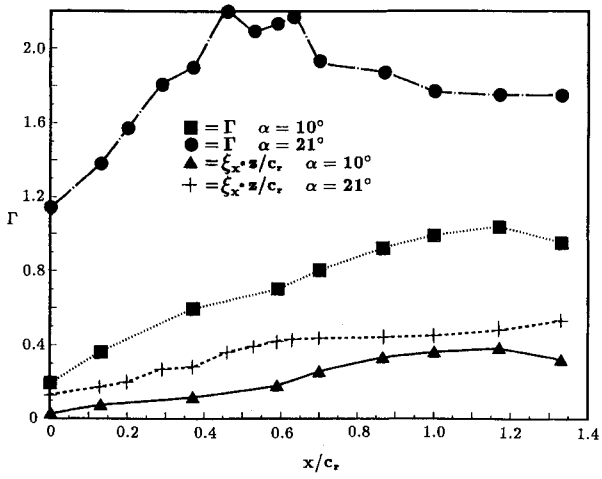

Fig. 9 Circulation and vorticity moment.

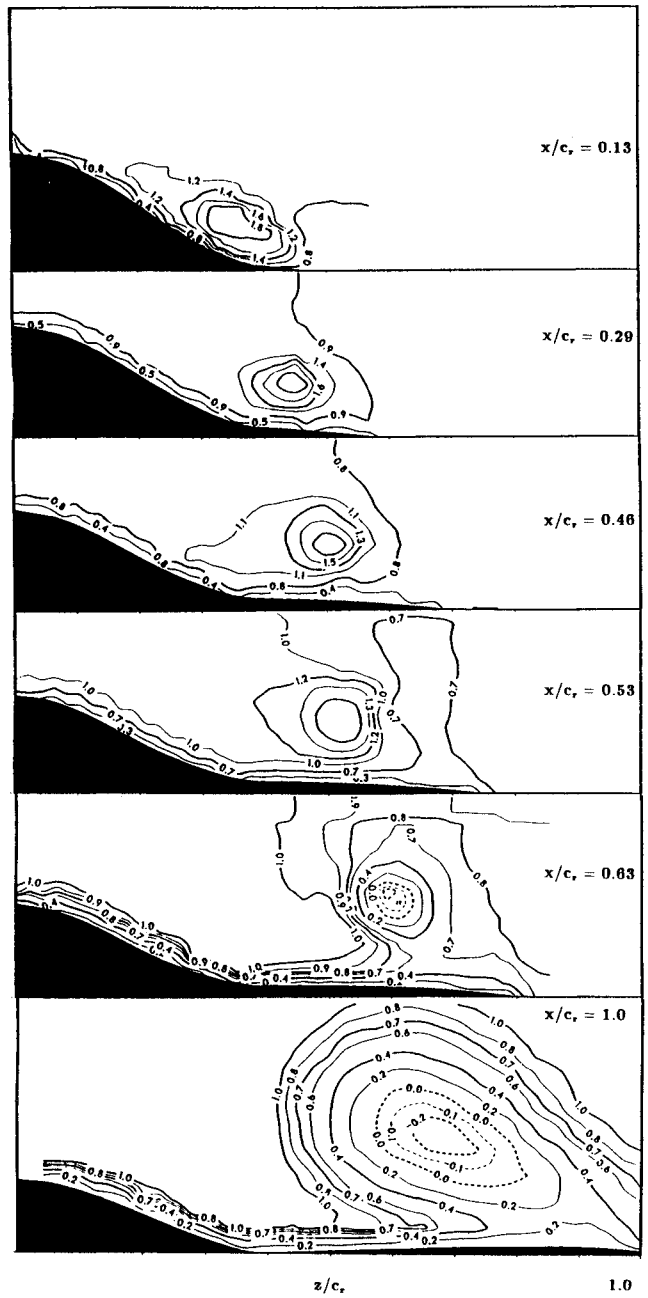

Fig. 10 Axial velocity U_x contours at α = 21 deg.

distance downstream. The positive circulation decreases downstream of the burst vortex location for the high angle-of-attack case, since a stronger turbulent mixing between the interfaces of positive and negative regions of vorticity near the wing surface decreases the local integrated time average value of this quantity. Also shown in Fig. 9 is the first moment of vorticity from the (x, y) plane, which is proportional to the vertical momentum flux. The data at α = 21 deg show that the slope of this quantity is reduced near the trailing edge of the wing, which has a direct impact on the adverse pitching moment of the aircraft.

Axial Velocity Contours

Figure 10 shows the development of the chordwise axial velocity contours along the trajectory of the core at α = 21 deg. The breakdown was initiated near $x/c_r \simeq 0.59$, where the axial velocity contours show a distinct region of reverse flow that is plotted as dashed contours. Thereafter, the apparent recirculating flow region, defined by the time mean

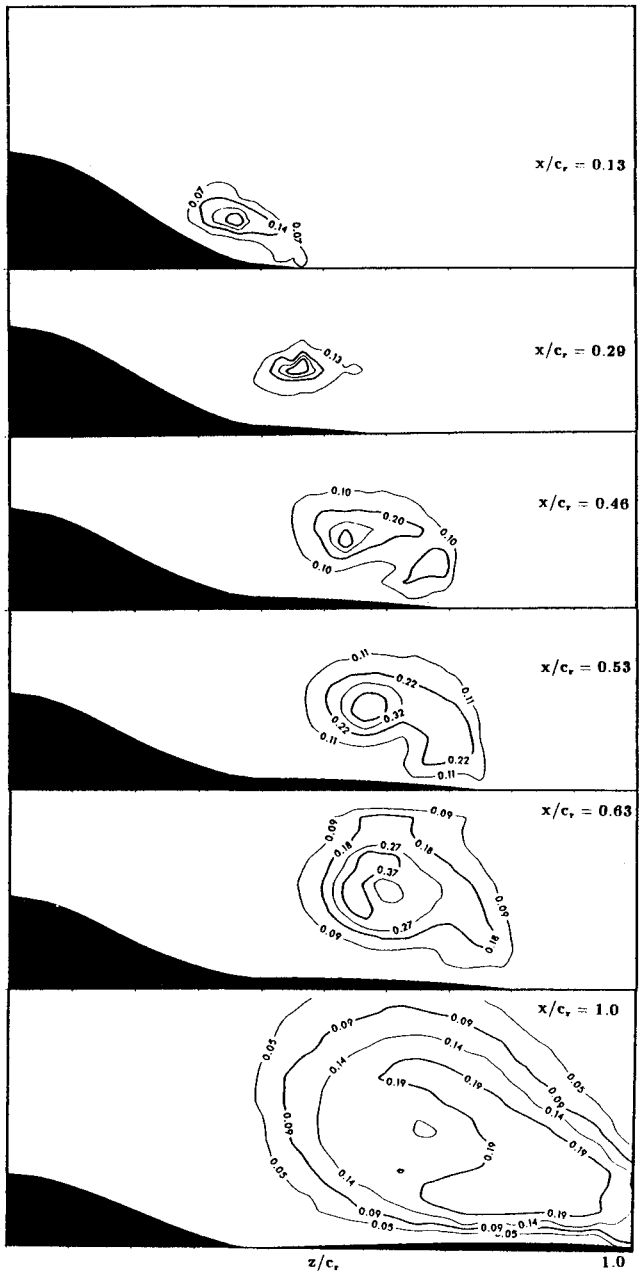

Fig. 11 Turbulent kinetic energy contours $\alpha = 21$ deg.

streamline encompassed in the interior region of the zero velocity contour, grows to a maximum diameter at $x/c_r = 0.87$. The maximum radius is 20% greater than the corresponding vortical radius r_ξ before the onset of the burst. The time mean reverse flow region terminates to form a finite recirculating zone in the near wake region at $x/c_r = 1.2$.

Turbulent Kinetic Energy Contours

Turbulent kinetic energy contours are shown in Fig. 11. The maximum turbulence levels coincide with the center core region of vorticity. The mean vortex velocity profile has an inflection instability that predicts a region at the core center that was always unstable to symmetric disturbances due to the local velocity gradients in this region. Although this instability may contribute to the turbulent energy production, it has limited use in predicting the onset of the burst location as defined by the stagnation point along the axial flow. The region of turbulent flow grows in a manner that reflects the intensity of the breakdown process after bursting, with turbulent kinetic energy levels on the order of 40%. The increased area of the turbulent zone beyond the burst location

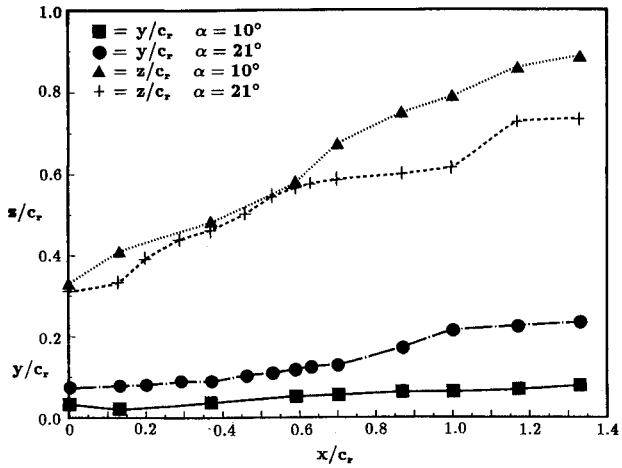

Fig. 12 Experimental vortex core coordinates.

at $x/c_r \simeq 0.59$ reflects the large-scale convection process of the energy-containing eddies and the dissipation of mean flow energy. Figure 12 shows the mean spatial vortex core locations relative to the fighter model orientation that was used in the transformation to the local vortex coordinates.

Background of the Vortex Stability Problem

There are two distinct forms of instability that have been observed by a host of investigators for the isolated single vortex flow problem. The experimental configurations have consisted of different upstream vorticity generators used to create a rotational flow bounded by the geometry of a cylindrical tube. The stability problem has been studied extensively in the past for axisymmetric flows utilizing the relevant stability analysis.[10-13] An excellent review article and bibliography is provided by Hall[14,15] and Leibovich,[16,17] where the authors discuss different spatial regimes during breakdown. The spiral instability that originates along the outer helical streamlines leads to large growth rates of nonsymmetric disturbances when a critical threshold is reached, where the production of turbulence is enhanced throughout the core of the vortex. The classical bubble breakdown is referred to as vortex burst since the physics of the flow change abruptly. This form of breakdown is characterized by both the sudden increasing of the diameter of the vortex core, and the formation of a stagnation point along the core axis with a recirculating flow region and enhanced turbulent mixing downstream. The hypothesis that vortex bursting is synonymous with two conjugate states where the approaching vortex flow is supercritical, and after bursting it is subcritical,[12,13] which suggests that the mean flow variables for the vortex flow problem should provide a threshold for the supercritical instability problem.

Examination of Vortex Spiral Instability Criterion

Whether a leading-edge vortex flow is stable to asymmetric disturbances depends on its internal flow structure, i.e., on the distribution of axial and circumferential velocities in the vortex core. A theory for the spiral instability of a leading-edge vortex was developed by Ludwieg.[11] The instability of the outer parts of the vortex core was proposed as an explanation for the vortex breakdown phenomenon. Ludwieg's stability theory for helical flows is an extension of Rayleigh's well-known stability criterion for rotating flows to allow for an additional axial velocity variation along the radial coordinate. It was shown by Ludwieg that a radial gradient of the axial velocity component has a destabilizing effect, so that an otherwise stable rotating flow can become highly unstable. Figure 13 shows the nomenclature for the conical vortex flow. The flow becomes locally unstable if the magnitudes of the nondimensional velocity gradients for a helical flow lie outside the solid lines depicted in Fig. 14. It was conjectured by Lud-

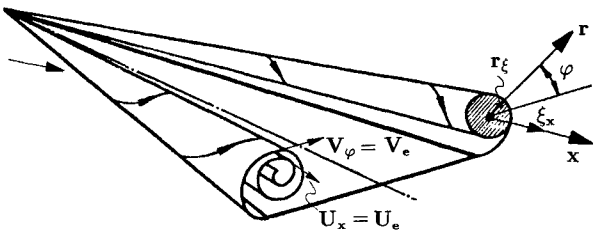

Fig. 13 Conical coordinate definition of vortex flow.

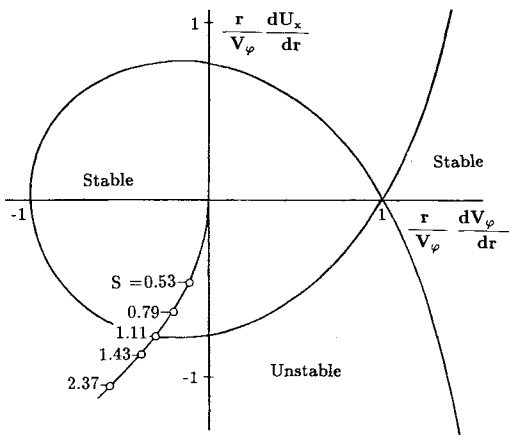

Fig. 14 Stability diagram from Ludwieg.[2,11]

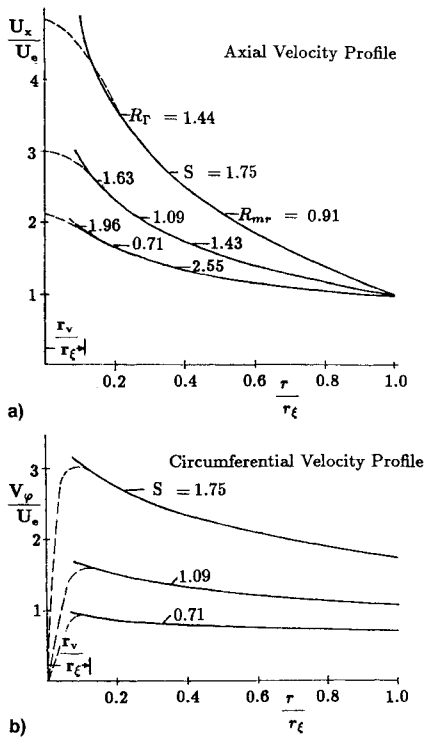

Fig. 15 a) Axial and b) circumferential velocity distribution.[14]

wieg that this criterion is approximately valid as a local stability criterion for any helical flow, i.e., that a flow becomes locally unstable if at any point in the vortex flowfield the criterion for the instability is satisfied.

Assuming that the vortex core is slender, i.e., its radius is small compared to the distance from the apex of the wing, the Euler equations provide a solution[14] for conical flow. It is assumed that the flowfield within the vortex core is axially symmetric and that the vorticity is continuously distributed, with the shear layer diffused. Both of these assumptions are good approximations to a realistic delta wing vortex. The following general solution for the velocity components in the axial U_x, circumferential V_φ, and radial V_r directions for conical flow outside the viscous subcore is

$$\frac{U_x}{U_e} = \left(1 - a\sqrt{\frac{r}{r_\xi}}\right) \qquad \frac{V_\varphi}{U_e} = S\sqrt{1 - (a^2/S^2)\sqrt{(r/r_\xi)}}$$
$$\frac{V_r}{U_e} = \frac{-a}{2}\frac{\delta r_\xi}{\delta x}\frac{r}{r_\xi} \tag{1}$$

where r_ξ is the local core radius encompassing the vorticity, and $a = (1 + 2S^2)^{1/2} - 1$. There are two parameters for the conical solution. The parameter $S = V_e/U_e$ is the magnitude of the velocity ratio at the outer edge of the vortex, whereas $(\delta r_\xi/\delta_x)$ as demonstrated in Fig. 7 represents the growth rate of the vortex boundary along the axis that depends on the aspect ratio of the delta wing. The velocity ratio S influences the velocity profile as a function of the radial coordinate as shown in Figs. 15a and 15b.

The radial velocity coordinate is negligible for small conical angles of the vortex flow and will be neglected in the stability comparison. When $S \geq 1.11$, the flow is unstable at the outer radial coordinate r_ξ, where the helix angle $\tan^{-1}(S)$ is ≥ 48 deg. The viscous subcore was derived by Hall,[14] and is shown as the dotted line in Figs. 15a and 15b. The governing dimensionless parameters for the stability problem are the Rossby and Reynolds numbers. The Reynolds number based on the core radius at $x/c_r = 0.25$ was 3.5×10^4 for the experimental data. It is hypothesized that the vortex core flow is transformed by an adverse pressure gradient so that the resulting vortex velocity distribution belongs to the same class of flows given by Eq. (1), but with an increased value of S. Thus, an originally stable vortex core can become unstable when subjected to an adverse pressure gradient. Note that Eq. (1) was derived with a zero axial pressure gradient. After the onset of instability, the disturbance waves are amplified in such a way that the vortex becomes asymmetric, which accelerates the breakdown and the turbulence production. The above equations can be integrated throughout the vortex region to evaluate an average helix angle for Ludwieg's criterion relative to the experimental data. This technique was adopted because the vortex flow for a delta wing geometry is not necessarily symmetric, and the experimental data comparison would be more accurate if an averaging is performed relative to the analytical formulation. The vortex energy ratio is defined as

$$R_{mr} = \frac{\int_0^{r_\xi} U^2 r\, dr}{\int_0^{r_\xi} V_\varphi^2 r\, dr} = \left[\frac{(a^2/2) + a + 1}{a^2 + a}\right] \tag{2}$$

Hence, at $S \geq 1.11$, where the spatial average helix angle is expressed as $\tan^{-1}(1/\sqrt{R_{mr}})$ is ≥ 40 deg, or the stability criteria $R_{mr} \leq 1.39$. The integral is weighted at larger r values where the instability is located because of the dependence on the cross-sectional area. For the experimental data the integrated (axial/crossflow) energy is defined as

$$R_{mr} = \frac{\int\int_{A_\xi} U_x^2\, dy\, dz}{\int\int_{A_\xi} (V^2 + W^2)_\xi\, dy\, dz} \tag{3}$$

where the area of integration A_ξ is defined from the finite domain bounded by the boundary of axial vorticity. For the data presented in this report the boundary is defined at a cutoff value of 6% of the local maximum vorticity value ξ_x in a (y, z) measurement plane. A plot of R_{mr} is shown for three

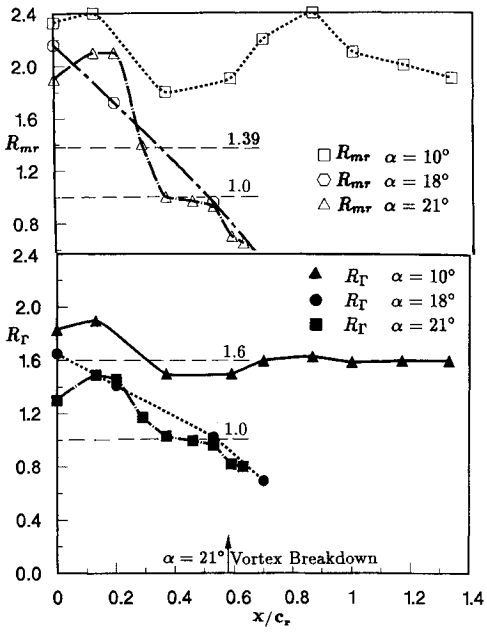

Fig. 16 Energy ratio and Rossby number vs x/c_r.

data sets in Fig. 16. The 10-deg angle-of-attack case is significantly above this threshold, and no reverse flow is evident, even though a significant increase of the core radius is apparent, indicating a growth of an instability. For the case with 21- and 18-deg angles of attack of the model, this parameter approaches $R_{mr} \simeq 1.0$ at the onset of the apparent vortex burst.

A Rossby number was defined[18] as the axial velocity divided by the maximum circumferential velocity at the radius r_v of the vortex viscous core. This parameter was successful in correlating vortex instability from numerical calculations for a wingtip vortex:

$$R_\Gamma = \frac{U_c}{V_\varphi(r_v)} = \frac{U_c 2\pi r_v}{\Gamma_v} = \left[\frac{1 - a \sin^{-1}(r_v/r_\xi)}{S\sqrt{1 - (a^2/S^2)}\sin^{-1}(r_v/r_\xi)}\right] \quad (4)$$

Since $U_c \to \infty$ as $r \to 0$ for the analytical model, the outer solution was evaluated at the numerical value of $(r_v/r_\xi) \simeq 0.15$, where the solution outside the viscous subcore matches closely to the local centerline velocity in the experimental data[18] of the full viscous problem. The (r_v/r_ξ) value is a weak function of the local Reynolds number if the Reynolds number is large. Hence, at $S \geq 1.11$, the stability criteria is $R_\Gamma \leq 1.6$. R_Γ does not vary significantly with a change in S, as shown in Figs. 15a and 15b. The radius and circulation increase at the same rate with a decrease in the centerline velocity, hence, this parameter has a gradual slope. For the experimental data the radius and mean circulation were obtained from the integrated area and vorticity, respectively, in the region r_v. The Rossby number R_Γ is plotted vs the dimensionless distance downstream in Fig. 16. This parameter approaches a value $R_\Gamma \simeq 1.0$ at the onset of the breakdown. The Rossby number reported for the average trend of the data[19] was for $R_\Gamma \simeq 1.0$ for the breakdown of delta wing vortices.

Examination of Vortex Burst Criterion

In this section an examination of the hypothesis proposed by Benjamin for vortex burst is analyzed in terms of the mean flow variables. Benjamin's formulation does not imply instability in the traditional sense of a disturbance growing in the temporal domain. Benjamin's analysis is similar to the hydraulic jump problem for open channel flow or a shock in compressible flow where the flow is supercritical upstream and transitions through an entropy increase to a subcritical state downstream. Like the hydraulic jump, the vortex flow has a larger cross-sectional area as noted in Fig. 7 after the transition, with an increase in the entropy through turbulence production. Hence, a vortex model is presented in terms of the mean flow variables to examine the criteria that the minimum specific mechanical energy flux[20] in the viscous subcore separates two distinct conjugate states of the flow. The analysis of the conical vortex flow by Hall is used in conjunction with a Rankine velocity distribution for the viscous subcore. A suitable choice of radius r_v/r_ξ interconnects the two solutions. The core axial velocity $U_c(x)$ is specified as uniform in the radial direction, and the crossflow component V_φ has the following radial variation in relationship to the circulation Γ_v in the viscous subcore:

$$V_\varphi = \frac{\Gamma_v r}{2\pi r_v^2} \qquad r \leq r_v$$
$$\frac{V_\varphi}{U_c} = S\sqrt{1 - (a^2/S^2)}\sin^{-1}(r/r_\xi) \qquad r_v < r \leq r_\xi \quad (5)$$

where Hall's Euler solution was used for the second term outside r_v. The dashed lines in Figs. 15a and 15b represent the inner solution, with U_c maintained as a constant that is a reasonable assumption in the viscous subcore. To evaluate the static pressure distribution the radial momentum equation $(\delta P/\delta r) = (\rho V_\varphi^2/r)$ was integrated. The static pressure variation in the viscous subcore can be expressed by the following:

$$P(r) = P_v - \frac{\rho\Gamma_v^2(r_v^2 - r^2)}{8\pi^2 r_v^4} \qquad 0 < r \leq r_v \quad (6)$$

where P_v in Eq. (6) is the static pressure evaluated at the juncture r_v/r_ξ. The energy equation along a streamline was applied from a point upstream to a point along the outer radius r_ξ to express the pressure at the outer streamline to the total freestream pressure $P_{r\infty}$ and the vortex-edge velocity. The static pressure variation that is valid outside the viscous subcore, i.e., $r_v < r \leq r_\xi$, is expressed by the following:

$$\frac{P(r)}{\frac{1}{2}\rho U_c^2} = \frac{P_{r\infty}}{\frac{1}{2}\rho U_c^2} - 2\left(\frac{U_c}{U_c}\right)^2\left[-\left(\frac{1}{2} + \frac{1}{a}\right)\sin^{-1}\left(\frac{r}{r_\xi}\right) + \frac{1}{2}\sin^{-2}\left(\frac{r}{r_\xi}\right) + \frac{1}{2}(1 + S^2)\right] \quad (7)$$

where P_v is evaluated at the juncture r_v/r_ξ in Eq. (7) to connect the outer to the inner analysis and is substituted in Eq. (6). The mechanical energy flux E inside the area defined by the radius r_v, neglecting the radial component of velocity, can be expressed by the following integral:

$$E = 2\pi\int_0^{r_v}\left[P + \frac{1}{2}\rho(U_c^2 + V_\varphi^2)\right]U_c r\, dr \quad (8)$$

The mass flow rate is defined by $\dot{m} = (\rho U_c A_v)$, where the area is defined by the radius $r_v(x)$ in the viscous subcore. Integrating the above equation for E under the constraint that the axial velocity $U_c(x)$ is independent of r in the viscous subcore, simplifies to the expression:

$$E = \frac{1}{2}\dot{m}U_c^2 + \dot{m}[(P_v/\rho) - (\Gamma_v^2/16\pi A_v)] \quad (9)$$

Define $U^* = (\Gamma_v^2/8\pi A_v U_c)$, which has units of velocity, and the last term in the brackets becomes $U_c U^*/2$. The circulation and volume flow $(A_v U_c)$ are considered to vary in the axial distance downstream for this local analysis.

The parameter $e = E/\dot{m}$ represents the specific energy, and the first term is expressed as $U_c^2 = [(U_c - U^*)^2 + 2U_c U^*$

$- U^{*2}]$. This equation can be normalized by dividing by $\frac{1}{2}U^{*2}$, and the specific energy per unit circulation and volume flow in the area bounded by r_v becomes

$$e_n = \left(\frac{P_{t\infty}}{\frac{1}{2}\rho U^{*2}} - 1\right) + \left(\frac{U_c}{U^*} - 1\right)^2 + \left(\frac{U_c}{U^*}\right) + 2\left(\frac{U_c}{U^*}\right)^2\left(\frac{U_e}{U_c}\right)^2\left[\left(\frac{1}{2} + \frac{1}{a}\right)\sin^{-1}\left(\frac{r_v}{r_\xi}\right) - \frac{1}{2}\sin^2\left(\frac{r_v}{r_\xi}\right) - \frac{1}{2}(1 + S^2)\right] \quad (10)$$

The normalized specific energy in the viscous subcore e_n is a multivalued function of (U_c/U^*) and the outer parameter S, which is characteristic of the supercritical state. The circulation in the viscous subcore is defined as $\Gamma_v = [2\pi r_v V_\varphi(r_v)]$, from Stoke's theorem. Substituting these values for the variable U^*, the following ratio $(U_c/U^*) = 2(U_c/V_{\varphi v})^2$ results. The minimum in the specific energy occurs when the addition of the last three terms in Eq. (10) are zero. It can be shown that these terms are a unique function of the outer variable $S = V_e/U_e$, once r_v/r_ξ is specified. The minimum of e_n occurs at $S = V_e/U_e = 1.58$ for the choice of $r_v/r_\xi = 0.15$, and $S = V_e/U_e = 1.5$ for $r_v/r_\xi = 0.1$, demonstrating a weak dependence on this parameter, which is a function of the Reynolds number. For the inner variables the quantity $(U_c/U^*) = 4.33$, which correlates to the velocity ratio $(U_c/V_{\varphi v}) = 1.47$, as compared to the outer velocity ratio $(U_c/V_c) = 0.63$, both values representing the minimum specific energy.

It is hypothesized that the value of $S \simeq 1.54$ represents the threshold between super and subcritical flow, which implies the maximum entropy state for the viscous subcore flow. The outer helix angle at r_ξ is 57 deg, and the inner subcore helix angle at r_v is 34 deg. If this flow is considered to be analogous to the hydraulic jump problem, then the value of $S \simeq 1.54$ delineates between two branches or solutions where the flow is supercritical and subcritical. Hence, at $S \leq 1.54$, the flow is supercritical, and the closer the flow approaches this value the more violent the transition and increase in entropy as the flow transforms to a vortical flow of larger radius that represents the conjugate subcritical state. Relative to the experimental data, the ratio expressed by Eq. (3) when $S = 1.54$ correlates to a threshold that is equivalent to $R_{mr} \geq 1.0$, and the average helical angle throughout the vortex flow is defined as $\tan^{-1}(1/\sqrt{R_{mr}})$ is ≤ 45 deg. R_{mr} represents the ratio of axial energy to the crossflow energy in the area bounded by the radius r_ξ. Hence, when $R_{mr} > 1$, the flow is supercritical, and when $R_{mr} \leq 1$, the flow is subcritical. A plot of R_{mr} is shown for three data sets in Fig. 16. All the cases shown are in the supercritical region. For the 10-deg angle-of-attack case, R_{mr} decreases and then levels off. However, a significant increase of the core radius was apparent from Fig. 7, indicating a transition to the subcritical flow. For the case with 21- and 18-deg angles of attack of the model, stagnation along the core center was evident with reverse flow in the core region and the energy ratio parameter approaching $R_{mr} \simeq 1.0$ at the onset of the apparent vortex burst. If an adverse pressure gradient is imposed on the vortex flow that is originally supercritical, it will effect the axial momentum flux with less impact on the rotational energy since the circulation increases gradually downstream, hence, the parameter S will increase toward the critical value.

These data sets embody the physics of vortex dynamics leading to vortex breakdown. Although the forebody/wing vortex-flow of fighter aircraft is inherently a more complex flow than the specific case formulated by a symmetric vortex flow study, the main thesis of stability arguments is generally applicable for vortex flows undergoing the instability transition.

Conclusions

Experimental data from a three-dimensional laser velocimeter have been analyzed for a chined forebody fighter configuration for two separate angles of attack. Force and moment data throughout an angle-of-attack range of 21 deg demonstrate the trends of the interaction of the vortex flow with the control surfaces. The nonintrusive LDV measurements of the velocity field provide a data set for the case of vortex breakdown. The measured velocity vectors were rotated from the tunnel coordinate system to the vortex axis coordinates to examine the relevant parameters for vortex instability. The swirl velocity ratio parameter S and the R_{mr} based on the axial-to-crossflow energy ratio provide for a parameter for the evaluation of the onset of breakdown. The energy ratio was defined from integrated parameters of the vortex flow and compared to theoretical arguments regarding vortex stability.

1) When $S \geq 1.11$ or $R_{mr} \leq 1.39$, the growth of the spiral instability leads to a dissemination and growth rate of the vortex core. This can be categorized as a turbulent dissipation of mean flow energy and an increase of the turbulent wake downstream. This instability provides an initial perturbation for the flow and may be the precursor to the breakdown of the supercritical vortex flow.

2) When $S \leq 1.55$ or $R_{mr} \geq 1.0$, the viscous subcore flow is supercritical, and as the energy ratio parameter $R_{mr} \rightarrow 1.0$, the transition from super to subcritical is imminent and the flow transitions to the classical stagnation point at the core center with a reverse flow region and with an amplification of the turbulence downstream, which represents a more violent transition process.

The vortex flow inside a tube and the flow generated by the shear layer over a delta wing show a similarity in the breakdown process. The spiral instability represents the initial instability for a turbulence production with increasing entropy that may accelerate the flow through the supercritical to subcritical transition state. These parameters provide a condition or threshold that is consistent with the experimental data.

Acknowledgments

This research was sponsored by the Air Force Office of Scientific Research/AFSC, U.S. Air Force, under Contract F49620-88-C-0053. I am indebted to my former colleagues in the experimental Aerodynamics Group at LASC-Georgia, W. A. Bell, C. J. Novak, C. R. Huie, and R. J. Englar. The experimental LDV data acquisition was supported under the LASC-Georgia IRAD program.

References

[1]Erickson, G. E., Rogers, L. W., Schreiner, J. A., and Lee, D. G., "Subsonic and Transonic Vortex Aerodynamics of a Generic Forebody Strake-Cropped Delta Wing Fighter," AIAA Paper 88-2596, June 1988.

[2]Wedemeyer, E. H., "Stable and Unstable Vortex Separation," *High Angle of Attack Aerodynamics*, AGARD CP 247, 1978.

[3]Skow, A. M., Titiriga, A., and Moore, W. A., "Forebody/Wing Vortex Interactions and Their Influence on Departure and Spin Resistance," *High Angle of Attack Aerodynamics*, AGARD CP-247, 1978.

[4]Skow, A. M., and Peake, D. J., "Control of the Forebody Vortex Orientation by Asymmetric Air Injection," AGARD CP-262-15, 1979.

[5]Peake, D. J., Owen, F. K., and Johnson, D. A., "Control of Forebody Vortex Orientation to Alleviate Side Forces," AIAA Paper 80-0183, Jan. 1980.

[6]Visser, K. D., Iwanski, K. P., Nelson, R. C., and Ng, T. T., "Control of Leading Edge Vortex Breakdown by Blowing," AIAA Paper 88-0504, Jan. 1988.

[7]Novak, C. J., and Huie, C. R., "3-D Laser Velocimeter Investigations of a Generic Fighter Flow-Field," AIAA Paper 87-0331, Jan. 1987.

[8]Ericsson, L. E., and Reding, J. P., "Dynamic Support Interfer-

ence in High Alpha Testing," *Journal of Aircraft*, Vol. 23, No. 12, 1986, pp. 889–896.

[9]Ericsson, L. E., and Reding, J. P., "Another Look at High Alpha Support Interference," *Journal of Aircraft*, Vol. 28, No. 5, 1991, pp. 584–591.

[10]Squire, H. B., "Analysis of the Vortex Breakdown Phenomena," Aeronautical Dept. Rept., Vol. 102, Imperial College, London, 1960.

[11]Ludwieg, H., "Vortex Breakdown," Deutsche Luft und Raumfahrt FB 70-40, Deutsche Forschungs und Versuchsanstalt fur Luft und Raumfahrt, Aerodynamische Versuchsanstalt Göttingen, Germany, Sept. 1970.

[12]Benjamin, T. B., "Theory of Vortex Breakdown Phenomenon," *Journal of Fluid Mechanics*, 14, 1962, pp. 593–602.

[13]Benjamin, T. B., "Some Developments in the Theory of Vortex Breakdown," *Journal of Fluid Mechanics*, 28, 1967.

[14]Hall, M. G., "A Theory for the Core of a Leading Edge Vortex ," *Journal of Fluid Mechanics*, Vol. 11, 1961.

[15]Hall, M. G., "Vortex Breakdown," *Annual Review of Fluid Mechanics*, Vol. 4, 1972.

[16]Leibovich, S., "The Structure of Vortex Breakdown," *Annual Review of Fluid Mechanics*, Vol. 10, 1978, pp. 221–246.

[17]Leibovich, S., "Vortex Stability and Breakdown: Survey and Extension," *AIAA Journal*, Vol. 22, No. 9, 1984, pp. 1192–1206.

[18]Powell, K. G., and Murman, E. M., "A Model for the Core of a Slender Viscous Vortex," AIAA Paper 88-0503, Jan. 1988.

[19]Spall, R. E., Gatski, T. B., and Grosch, C. E., "A Criteria for Vortex Breakdown," *Physics of Fluids*, Vol. 30, Nov. 1987, pp. 3434–3440.

[20]Landahl, M. T., and Widnall, S. E., "Vortex Control," NASA Symposium on Aircraft Wake Turbulence, Sept. 1970, pp. 137–155.